# Depth and Bathymetry of Supraglacial Melt Ponds from Remote Sensing Observations

Michela Savignano[a,b], Alison F. Banwell[b], and Waleed Abdalati[a,b]
[a]University of Colorado Boulder, Department of Geography, [b]Cooperative Institute for Research in Environmental Sciences (CIRES)
Contact: michela.savignano@colorado.edu

## Objectives

1. Determine the best method for calculating water depth from high resolution multispectral Worldview-2/3 imagery, validated with ICESat-2
2. Demonstrate that paired WorldView-2/3 imagery and ArcticDEM strips can be used to calculate bathymetry and incision rate in surface water features

Long Term Objective: Calculate incision rates in the Petermann river channel to constrain the conditions necessary to form and maintain an ice-shelf estuary

## Study Area

### Petermann Ice Shelf, Greenland 81° N, 61° W

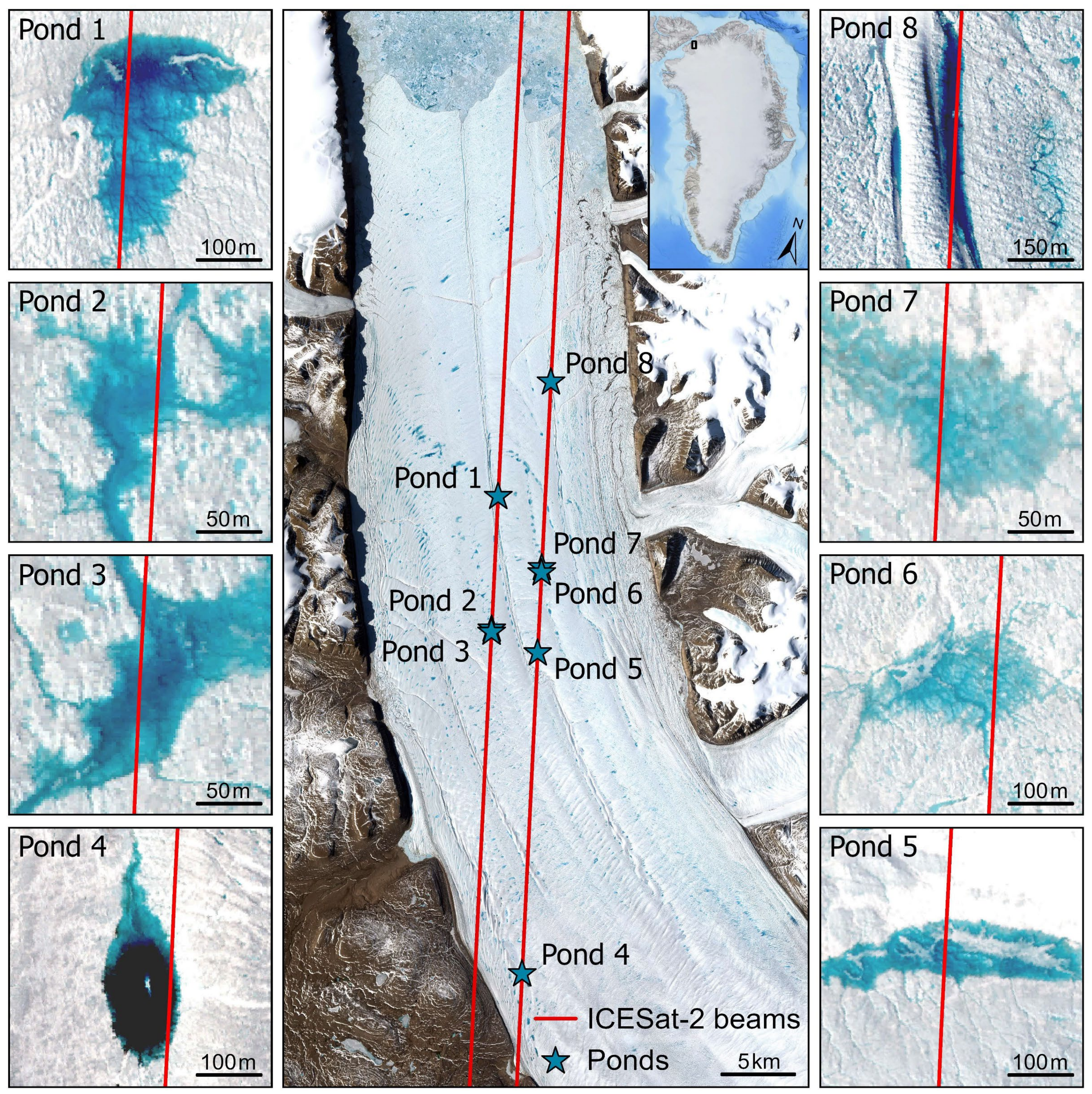


**Figure 1** – Sentinel-2 image of Petermann Ice Shelf with locations of ponds and ICESat-2 beams. Inset map shows the location of Petermann outlined in black. WorldView-2 images of ponds 1-8 (copyright Maxar 2023) are shown with corresponding ICESat-2 beams in red.

## Data

**Table 1** – Data products and acquisition information.

| Satellite | Product(s) | Acquisition Date & Time | Resolution | Revisit |
|---|---|---|---|---|
| WorldView-2 | Multispectral imagery, ArcticDEM | 2023-06-27 18:58:54 UTC | 2 m | <1 day |
| ICESat-2 | ATL03 geolocated photon cloud | 2023-06-29 08:43:30 UTC | 4 mm | 91 days |

## Depth Equations

**Table 2** – Equations for calculating depth from optical imagery. *Calibrated values from Moussavi et al. (2016). C = coastal blue, B = blue, G = green, Y = yellow, R = red, E = red edge.

| Method | Equation | Bands ($R_\lambda$) | Citation |
|---|---|---|---|
| Radiative Transfer (RT) | $D = \frac{\ln(A_d - R_\infty) - \ln(R_\lambda - R_\infty)}{g}$ | R, G, B | Philpot (1989)* |
| Dual Channel (DC) | $D = a\left(ln\left[\frac{R_{\lambda_1}}{R_{\lambda_2}}\right]\right)^2 + b\left(ln\left[\frac{R_{\lambda_1}}{R_{\lambda_2}}\right]\right) + c$ | G-R, Y-R, G-Y, B-R, C-R, B-Y, C-Y, B-G | Legleiter et al. (2009)* |
| Single Channel (SC) | $D = \propto_0 \frac{1}{R_\lambda + \propto_1} + \propto_2$ | R, G, B, C, Y, E | Box and Ski (2007)* |
| Power Law (PL) | $D = 0.2764 R_\lambda^{-0.8952}$ | R | Williamson et al. (2018) |
| Exponential Law (EL) | $D = 14.9572 e^{-4.2629 R_\lambda} + 0.5242$ | G | Lutz et al. (2024) |
| Refraction Correction (RC) | $D = z_b - 1.33 z_w$ | DEM | Chudley et al. (2019) |

## Depth & Bathymetry Methods

### WorldView-2 & ArcticDEM

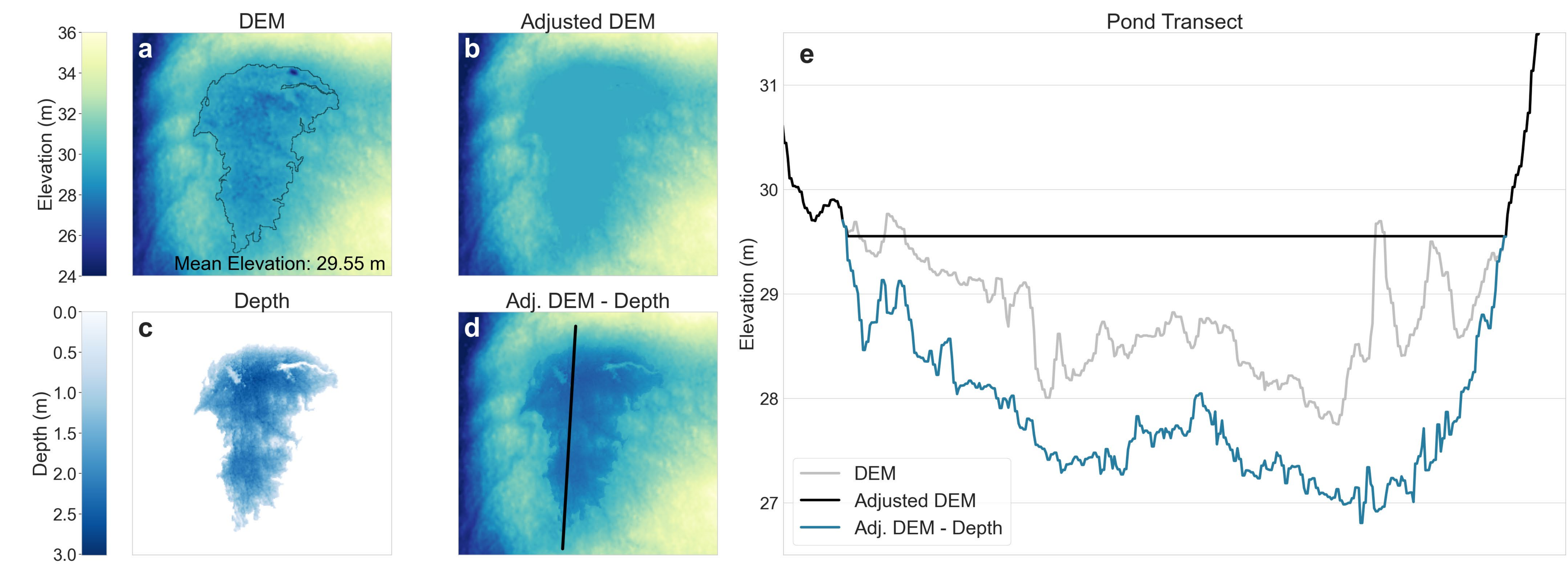


**Figure 2** – Steps used to calculate depth and bathymetry from paired WV-2 scenes and ArcticDEM strips for Pond 1: (a) DEM with pond marginal pixels and mean marginal elevation in black, (b) adjusted DEM with smoothed water surface equal to the mean marginal elevation, (c) water depth calculated from WV-2 reflectance (Table 2), (d) pond basin bathymetry, calculated by subtracting water depth from the adjusted DEM, with ICESat-2 transect in black, and (e) profiles of pond data in a, **b**, and **d** along an ICESat-2 transect.

### ICESat-2

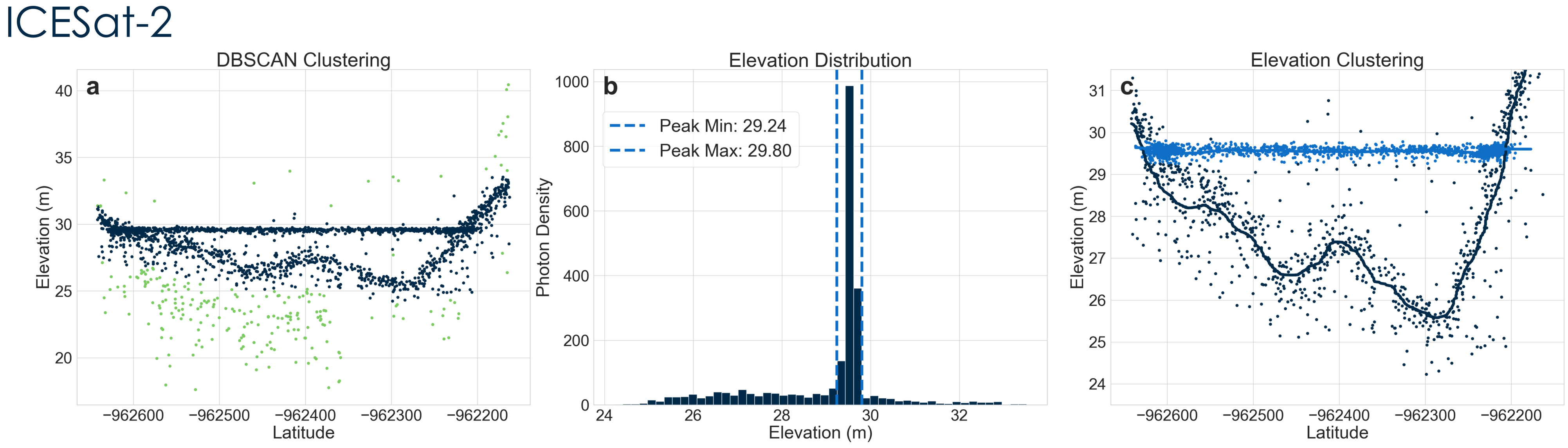


**Figure 3** – Steps used to calculate depth and bathymetry from ICESat-2 photons for Pond 1: (a) DBSCAN clustering to remove low density photons, (b) histogram of remaining **high density photon** elevations, and (c) clustering based on elevation histogram peak, with moving averages calculated for the **air-water interface** and the **water-ice interface.**

## Depth & Bathymetry Results

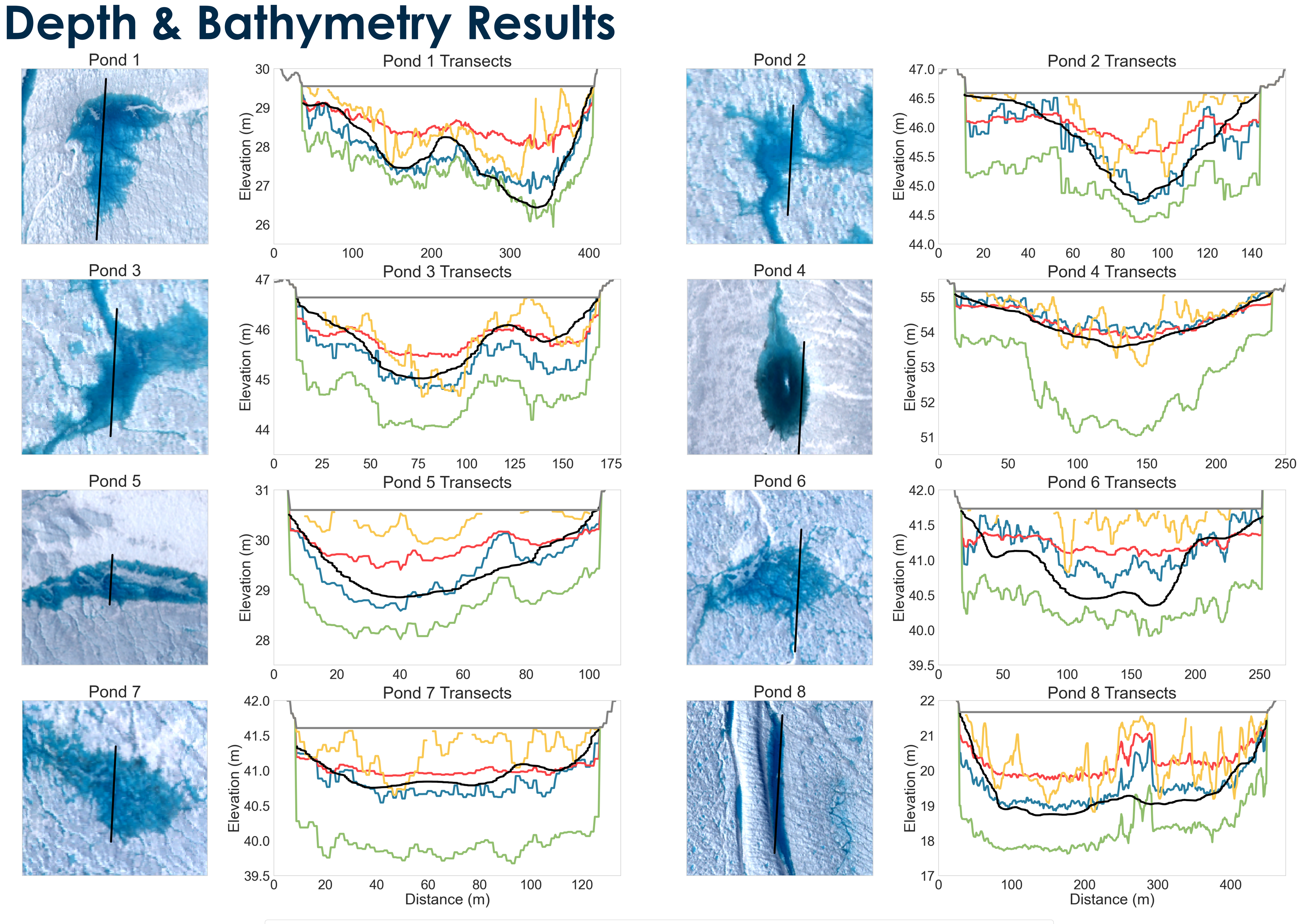


**Figure 4** – Depth transects for all ponds calculated with **ICESat-2** and the optimal band combinations for each the four methods that calculate depths > 0 m across all ponds: **PL (R)**, **EL (G)**, **DC (B-G)**, and **RC (DEM)** (Table 2). The black lines on the WorldView-2 pond images show the portions of the ICESat-2 transects that are plotted on the right. Imagery © 2023 Maxar.

## Validation Metrics

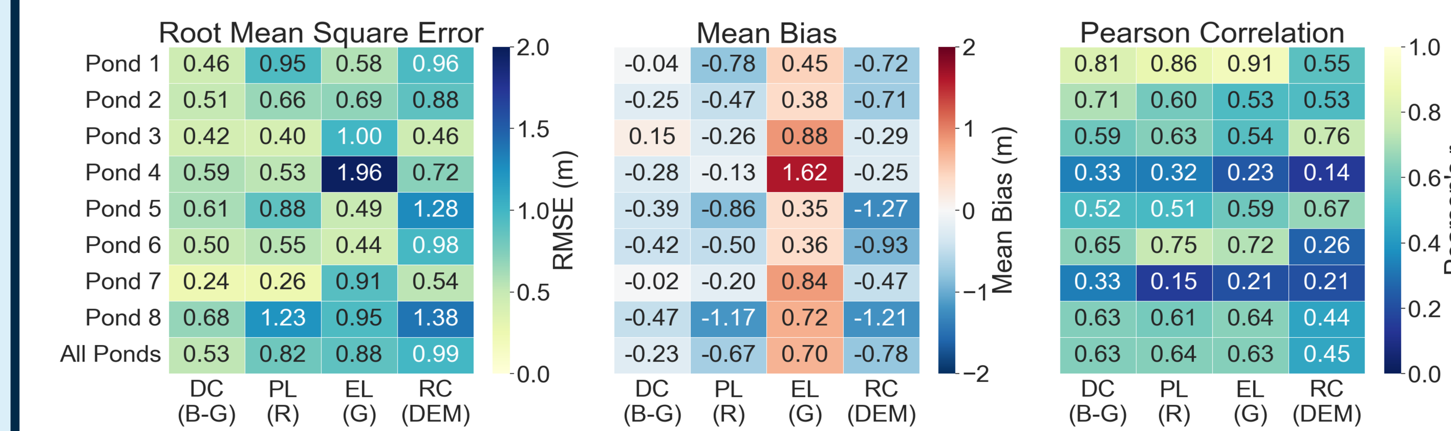


**Figure 5** – Heatmaps of RMSE, mean bias, and Pearson correlation for all ponds, individually and in aggregate, for the four best water depth methods when compared to ICESat-2 profiles.

## WorldView-2 Reflectance vs. Depth

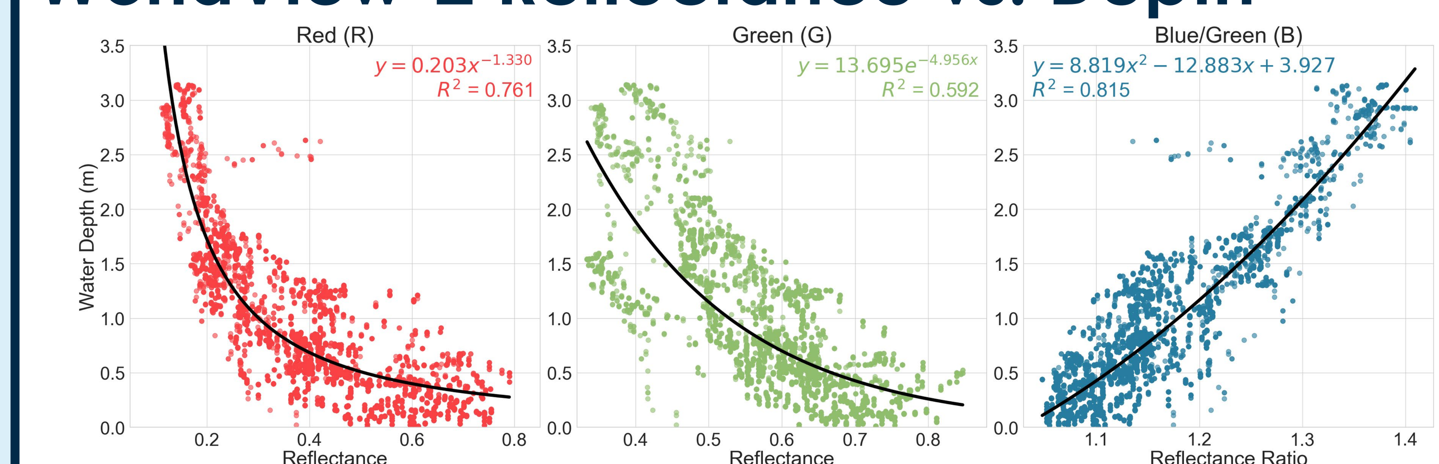


**Figure 6** – ICESat-2 derived depths vs. WorldView-2 reflectance in the **red** and **green** bands, and the **blue/green** band ratio, with best fit lines in black.

## Conclusions

1. The Dual Channel (DC) method using the blue/green band ratio produces the most accurate modeled meltwater depths from WorldView-2 imagery
2. The Power Law (PL) and Exponential Law (EL) methods, originally calibrated for Sentinel-2 imagery, can be used with WorldView-2 imagery to calculate depth and bathymetry but may require additional parameter tuning
3. Our novel method, validated against ICESat-2, uses paired optical images and corresponding DEMs to calculate water depth and bathymetry, providing greater spatial coverage and temporal resolution than ICESat-2 alone

## Petermann River Incision Rate

Mean Incision Rates: **2.4 cm/day** at the terminus and **0.6 cm/day** 500 m upstream

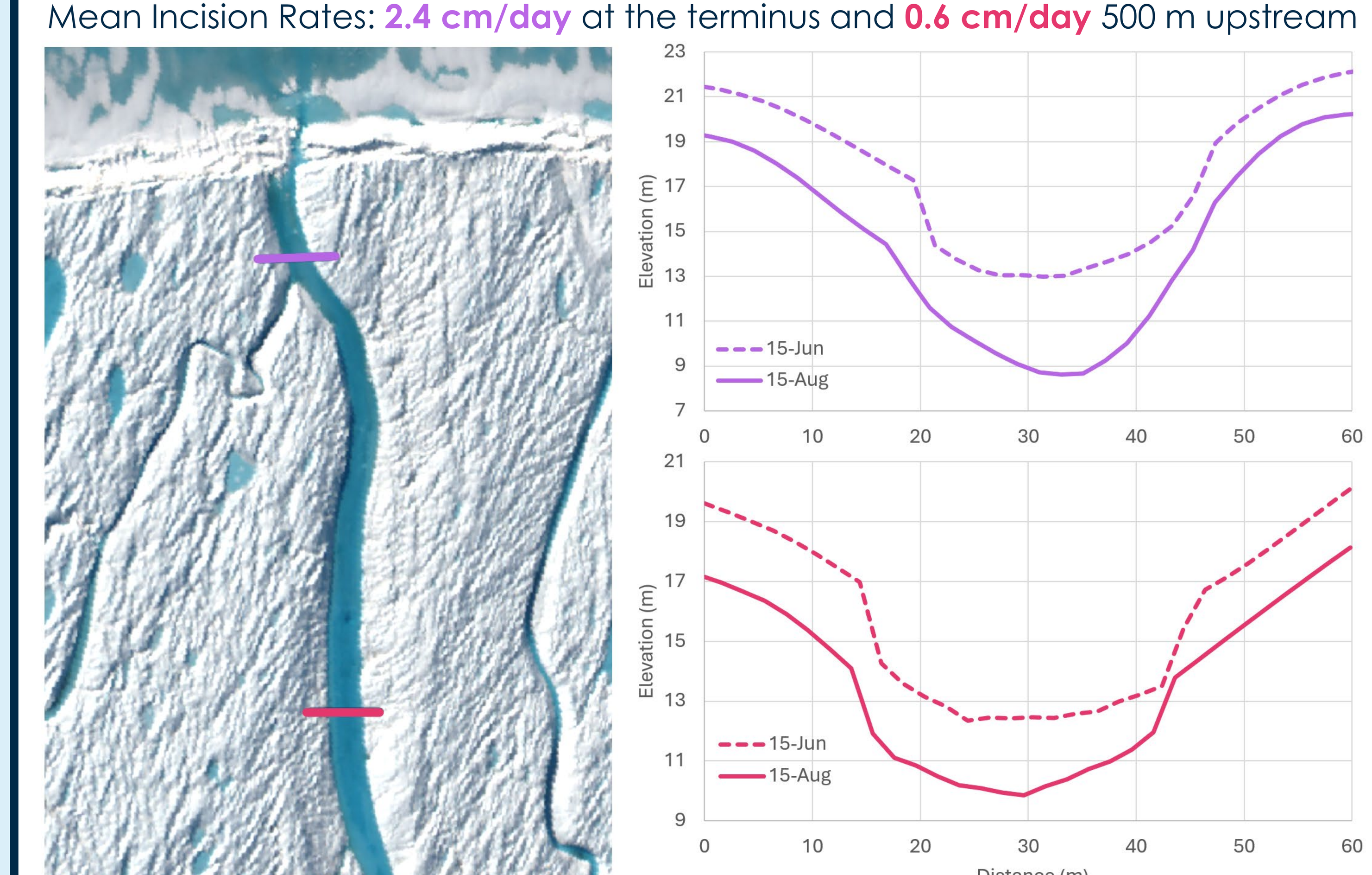


**Figure 7** – Channel bathymetry at two cross-sections of the Petermann river at the beginning (June 15) and end (August 15) of the 2016 melt season. Bathymetry is calculated from paired WorldView-3 imagery and ArcticDEM strips using the DC (B-G) method. Imagery © 2016 Maxar.

## References & Acknowledgements

Funding support was provided by NASA Cryosphere award #80NSSC24K0311 and NSF-OPP award #1841607 (PI Banwell). Geospatial support for this work provided by the Polar Geospatial Center under NSF-OPP awards 1043681, 1559691, and 2129685. DEMs provided by the Polar Geospatial Center under NSF-OPP awards 1043681, 1559691, 1542736, 1810976, and 2129685.

1. Porter, C. et al. ArcticDEM - Strips, Version 4.1. Harvard Dataverse https://doi.org/10.7910/DVN/C98DVS (2022).
2. ATLAS/ICESat-2 L2A Global Geolocated Photon Data, Version 6. National Snow and Ice Data Center https://nsidc.org/data/atl03/versions/6 (2020).
3. Philpot, W. D. Bathymetric mapping with passive multispectral imagery. Appl. Opt., AO 28, 1569–1578 (1989).
4. Legleiter, C. J., Roberts, D. A. & Lawrence, R. L. Spectrally based remote sensing of river bathymetry. Earth Surface Processes and Landforms 34, 1039–1059 (2009).
5. Box, J. E. & Ski, K. Remote sounding of Greenland supraglacial melt lakes: implications for subglacial hydraulics. Journal of Glaciology 53, 257–265 (2007).
6. Williamson, A. G., Banwell, A. F., Willis, I. C. & Arnold, N. S. Dual-satellite (Sentinel-2 and Landsat 8) remote sensing of supraglacial lakes in Greenland. The Cryosphere 12, 3045–3065 (2018).
7. Lutz, K. et al. Assessing supraglacial lake depth using ICESat-2, Sentinel-2, TanDEM-X, and in situ sonar measurements over Northeast and Southwest Greenland. The Cryosphere 18, 5431–5449 (2024).
8. Chudley, T. R. et al. Supraglacial lake drainage at a fast-flowing Greenlandic outlet glacier. Proceedings of the National Academy of Sciences 116, 25468–25477 (2019).